JBC RESEARCH ARTICLE

# African swine fever virus pB475L evades host antiviral innate immunity *via* targeting STAT2 to inhibit IFN-I signaling

Received for publication, February 6, 2024, and in revised form, May 16, 2024 Published, Papers in Press, June 13, 2024,
https://doi.org/10.1016/j.jbc.2024.107472

**Zhao Huang**[1,2,3,‡], **Zhanzhuo Mai**[1,3,‡], **Cuiying Kong**[1], **Jianyi You**[1,3], **Sizhan Lin**[1,3], **Chenyang Gao**[1,3], **WenBo Zhang**[1,3], **Xiongnan Chen**[1,2,3], **Qingmei Xie**[4], **Heng Wang**[1,3,5], **Shengqiu Tang**[2], **Pei Zhou**[1,3,*], **Lang Gong**[1,3,*], and **Guihong Zhang**[1,5,6,7,*]

*From the* [1]*Key Laboratory of Zoonosis Prevention and Control of Guangdong Province, College of Veterinary Medicine, South China Agricultural University, Guangzhou, China;* [2]*Guangdong Provincial Key Laboratory of Utilization and Conservation of Food and Medicinal Resources in Northern Region, Shaoguan University, Shaoguan, China;* [3]*African Swine Fever Regional Laboratory of China,* [4]*College of Animal Science, and* [5]*Research Center for African Swine Fever Prevention and Control, South China Agricultural University, Guangzhou, China;* [6]*Maoming Branch, Guangdong Laboratory for Lingnan Modern Agriculture, Guangdong, China;* [7]*Key Laboratory of Animal Vaccine Development, Ministry of Agriculture and Rural Affairs, Guangzhou, China*

Reviewed by members of the JBC Editorial Board. Edited by Clare E. Bryant

**African swine fever virus (ASFV) causes severe disease in domestic pigs and wild boars, seriously threatening the development of the global pig industry. Type I interferon (IFN-I) is an important component of innate immunity, inducing the transcription and expression of antiviral cytokines by activating Janus-activated kinase–signal transducer and activator of transcription (STAT). However, the underlying molecular mechanisms by which ASFV antagonizes IFN-I signaling have not been fully elucidated. Therefore, using coimmunoprecipitation, confocal microscopy, and dual luciferase reporter assay methods, we investigated these mechanisms and identified a novel ASFV immunosuppressive protein, pB475L, which interacts with the C-terminal domain of STAT2. Consequently, pB475L inhibited IFN-I signaling by inhibiting STAT1 and STAT2 heterodimerization and nuclear translocation. Furthermore, we constructed an ASFV-B475L$^{7PM}$ mutant strain by homologous recombination, finding that ASFV-B475L$^{7PM}$ attenuated the inhibitory effects on IFN-I signaling compared to ASFV-WT. In summary, this study reveals a new mechanism by which ASFV impairs host innate immunity.**

African swine fever (ASF) is a highly lethal disease in pigs caused by infection with the ASF virus (ASFV) that has seriously impacted the pig industry in more than 50 countries (1). ASFV, the only member of the *Asfarviridae* family, is an enveloped icosahedral deoxyvirus (2); it is a linear double-stranded DNA virus with a genome range of 170 to 193 kbp. ASFV contains 151 to 167 tightly packed open reading frames (3) and can be divided into different genotypes according to the B646L gene 3′-end sequences. To date, 24 different ASFV genotypes have been identified in Africa (4, 5), and the predominant genotype circulating in Eurasia is the type II strain (6). As of 2023, ASF remains a pandemic in Eurasia, and ASF outbreaks are still being reported in new countries (7–9). To date, a safe and effective vaccine or anti-ASFV drug to contain the spread of ASF does not exist (10). Importantly, the emergence of genotype I and II recombinant ASFV in China poses a greater challenge to vaccine development (11). Therefore, the need to clarify the molecular mechanisms of ASFV for developing anti-ASF vaccines and drugs is urgent.

Innate immunity is the first line of defense against viral infection, and type I interferon (IFN-I), contained in almost any type of nucleated cell, is an important component of the innate immune response (12). Once secreted by a cell, IFN-I acts on itself or other cells and is first signaled by interferon-α/β receptor (IFNAR) to induce interferon-stimulated gene (ISG) expression through the Janus-activated kinase (JAK)–signal transducer and activator of transcription (STAT) signaling pathway (13). STAT2 is an essential component in the JAK–STAT signaling pathway, is recruited by IFN-α/β receptor, IFNAR2, and phosphorylated by JAK1. Moreover, interactions of STAT2 with JAK1 cause STAT2 phosphorylation and subsequent heterodimer formation with phosphorylated STAT1 (p-STAT1) *via* the Src homology 2 domain (SH2D) (14), which subsequently are translocated to the nucleus in association with interferon regulatory factor 9 (IRF9) (15–17), activating transcription of the antiviral cytokines by the interferon-sensitive response element (ISRE) promoter (18, 19). Heterodimerization is critical to the nuclear translocation of STAT because the nuclear localization signal is formed by a partially dimerized STAT DNA-binding domain (20).

ASFV induces IFN-I and ISG expression through the cyclic GMP–AMP synthase–stimulator of IFN genes and retinoic acid–inducible gene I signaling pathways (21, 22), but the induction level is lower than that of the Sendai virus, caused by the inhibition of IFN-I production and signal transduction through multiple pathways by ASFV (23). This phenomenon has been confirmed in a study that demonstrated the induction

‡ These authors contributed equally to this work.
* For correspondence: Guihong Zhang, guihongzh@scau.edu.cn; Lang Gong, gonglang@scau.edu.cn; Pei Zhou, zhoupei@scau.edu.cn.

of the innate antiviral response by attenuated ASFV strains (NH/P68) rather than virulent strains (Armenia/07) (24). Currently, attenuated ASFV gene deletion vaccines have emerged as the most promising vaccine candidates for ASF (25). MGF360-9L and MGF505-7R are key virulence genes that inhibit IFN-I signal transduction. Notably, the ASFVΔMGF360-9LΔMGF505-7R strain protects 83.4% of pigs in the same pen from the attack of parental strains (26, 27). Studies suggest that an IFN-I-mediated antiviral response is crucial to resist pathogen invasion and eliminate pathogens from the body, supporting the view that live attenuated vaccines are feasible for ASF containment (28, 29). Therefore, screening for ASFV proteins that potentially inhibit the immune response to IFN-I is crucial for developing ASF gene deletion vaccines. In addition, investigating the immunosuppressive mechanism of conserved proteins is more beneficial to developing vaccines and antiviral drugs against recombinant ASFV.

pB475L is a nonstructural protein encoded by ASFV that contains 475 amino acids, but its biological function is unclear. Therefore, this study investigated the immunosuppressive function and molecular mechanisms of pB475L to determine its potential as an ASF vaccine or an anti-ASFV drug target.

## Results

### *ASFV pB475L antagonizes IFN-I signaling*

Our previous study indiscriminately screened 149 ASFV proteins, finding that pB475L significantly inhibited IFN-I-activated ISRE promoter activity (27). This study confirmed that pB475L dose-dependently inhibited IFN-I-activated ISRE promoter activity (Fig. 1*A*); notably, we also found that pB475L inhibits Sendai virus active IFN-β and ISRE promoter activity (Fig. S1). Furthermore, ectopic expression of different pB475L doses did not affect cell viability (Fig. S2). ISG15 and ISG54 are

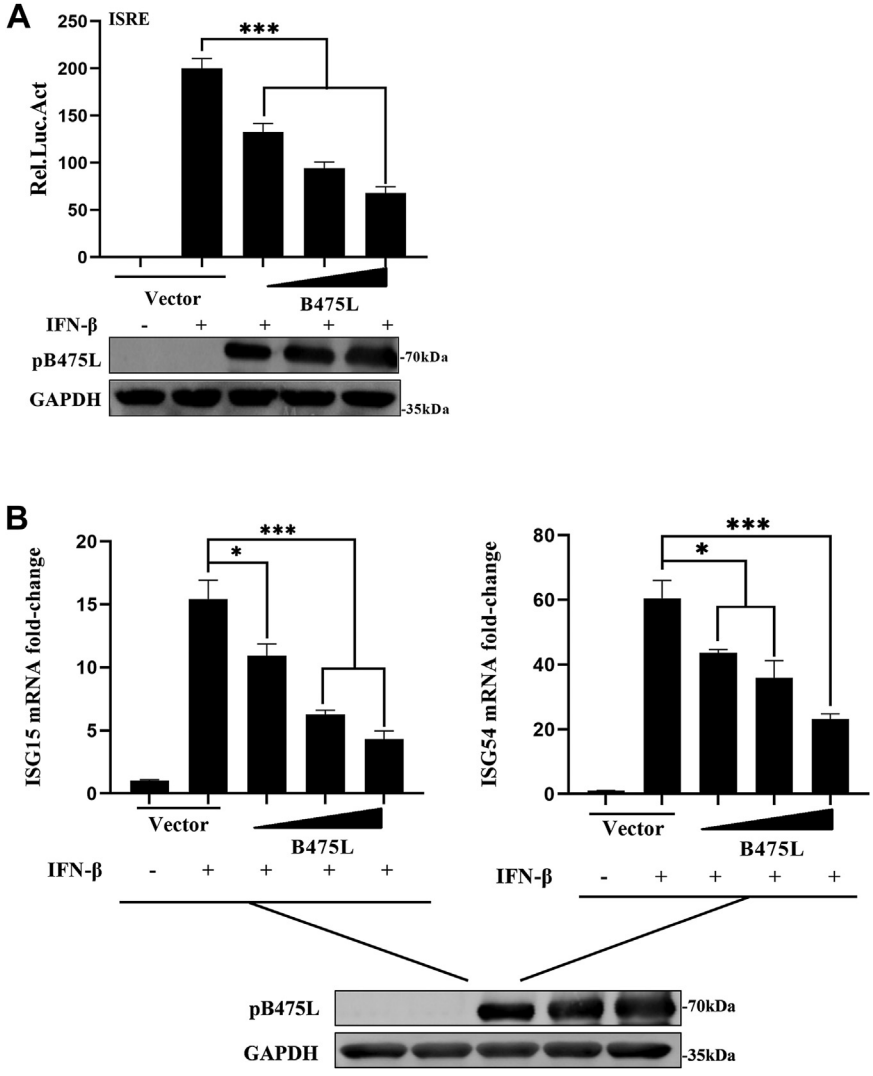


**Figure 1. ASFV pB475L antagonizes IFN-I signaling.** *A*, HEK293T cells cultured in 24-well plates were transfected with ASFV B475L expression plasmid or empty vector (100, 200, or 400 ng/well), pRL-TK (25 ng/well), and ISRE Luc (125 ng/well). After 24 h, the cells were treated with 1000 U/ml IFN-β for 8 h and analyzed by dual luciferase reporter. *B*, HEK293T cells cultured in 24-well plates were transfected with ASFV B475L expression plasmid or empty vector (100, 200, or 400 ng/well). After 24 h, cells were treated with 1000 U/ml IFN-β for 8 h and analyzed by quantitative PCR. *$p < 0.05$; **$p < 0.01$; ***$p < 0.001$. ASFV, African swine fever virus; HEK293T, human embryonic kidney 293T cell line; IFN-I, type I interferon; IFN-β, interferon beta; ISRE, interferon-sensitive response element.

important ISGs for IFN-I induction (30). Thus, we examined the transcriptional levels of several ISGs in cells ectopically expressing pB475L and treated with IFN-I to investigate whether pB475L regulates ISG transcription. Ectopic pB475L expression significantly and dose-dependently suppressed ISG15 and ISG54 mRNA transcription levels (Fig. 1*B*). These results suggest that pB475L antagonized IFN-I signaling.

### *pB475L suppresses IFN-I signaling downstream of STAT phosphorylation*

IFN-I signaling is induced by IFNAR binding, which elicits conformational changes between IFNAR1 and IFNAR2, leading to mutual phosphorylation of JAK1 and tyrosine kinase 2 (TYK2) (31, 32). After that, JAK1 induces STAT1 and STAT2 phosphorylation. To explore the key target proteins involved in IFN-I signaling that are antagonized by pB475L, we monitored IFN-I downstream protein expression 2 h after treatment with or without IFN-I *via* Western blot (WB). Four phosphoantibodies were used to detect the phosphorylation sites of JAK1 Tyr1034/1035, TYK2 Tyr1054/1055, STAT1 Tyr701, and STAT2 Tyr690. As expected, p-JAK, p-TYK2, p-STAT1, and p-STAT2 levels significantly increased after IFN-I treatment. Surprisingly, pB475L did not inhibit the expression and phosphorylation of any proteins in the JAK–STAT signaling pathway (Fig. 2, *A* and *B*), suggesting that pB475L suppresses IFN-I signaling downstream of STAT phosphorylation.

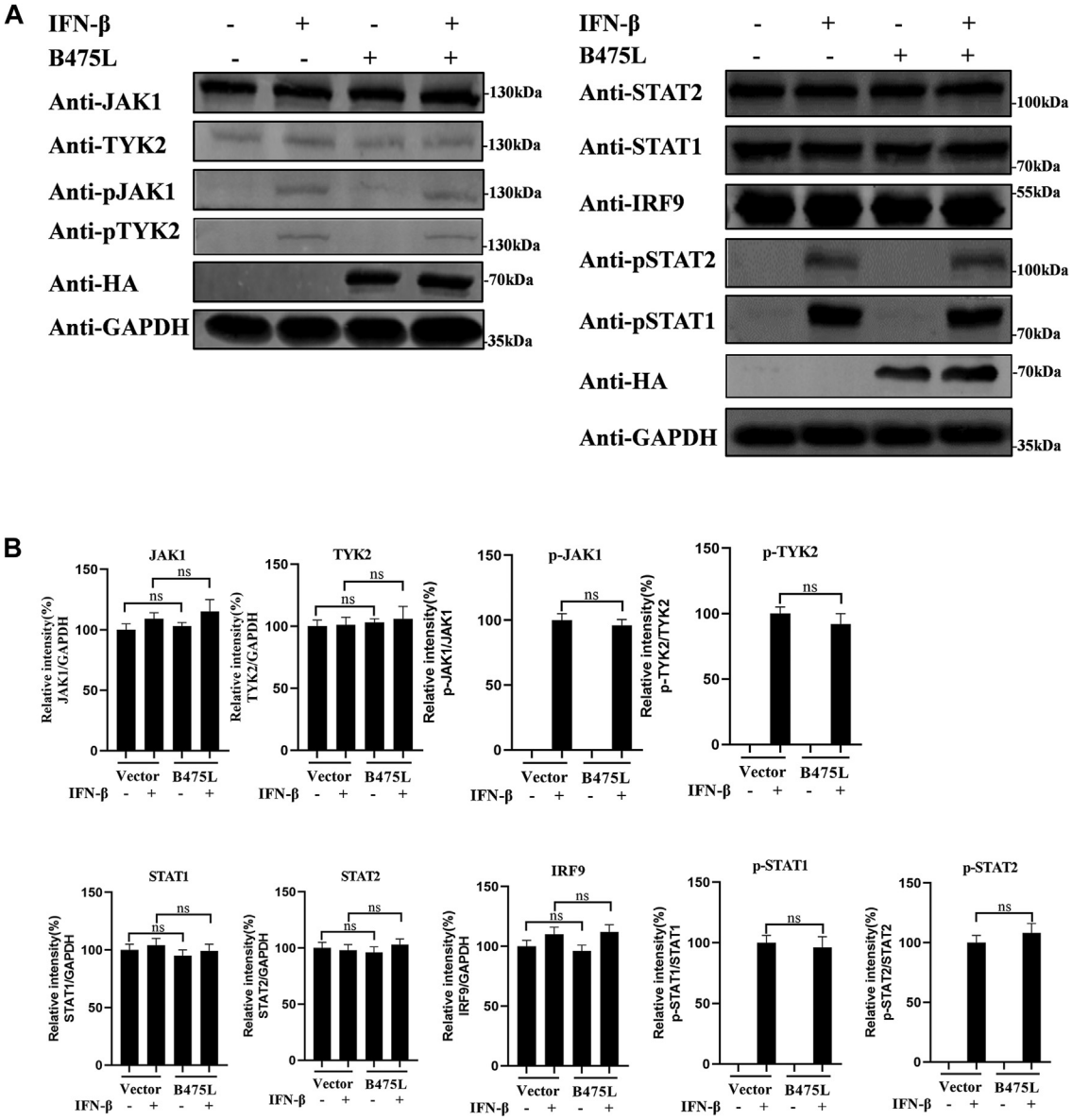


**Figure 2. pB475L does not affect the expression of key proteins in the JAK–STAT pathway.** *A*, HEK293T cells cultured in 12-well plates were transfected with ASFV B475L expression plasmid (1000 ng/well) for 24 h, followed by IFN-β (1000 U/ml) for 2 h. Protein expression was assessed by Western blot. *B*, the relative intensities of JAK1, TYK2, p-JAK1, p-TYK2, STAT1, STAT2, IRF9, p-STAT1, and p-STAT2 were quantified using Western blot with GAPDH as an internal control. ASFV, African swine fever virus; HEK293T, human embryonic kidney 293T cell line; IFN-β, interferon beta; IRF9, interferon regulatory factor 9; JAK, Janus-activated kinase; STAT, signal transducer and activator of transcription.

### *pB475L interacts with STAT2*

To explore the key targets of pB475L in antagonizing IFN-I signaling, hemagglutinin (HA)-tagged pB475L and DYKDDDDK (FLAG)-tagged JAK–STAT pathway proteins were cotransfected into human embryonic kidney 293T (HEK293T) cells. Coimmunoprecipitation (co-IP) was used to detect the interaction between exogenous pB475L and key proteins in the IFN-I pathway. pB475L interacted with STAT2 but not JAK1, TYK2, STAT1, or IRF9 (Fig. 3, *A* and *B*). For confirmation, we examined the interaction between pB475L and endogenous STAT2 by transfecting HA-tagged pB475L into cells, which were then immunoprecipitated using STAT2 antibody and HA; pB475L interacted with endogenous STAT2 (Fig. 3*C*). Finally, we assessed the subcellular localization of

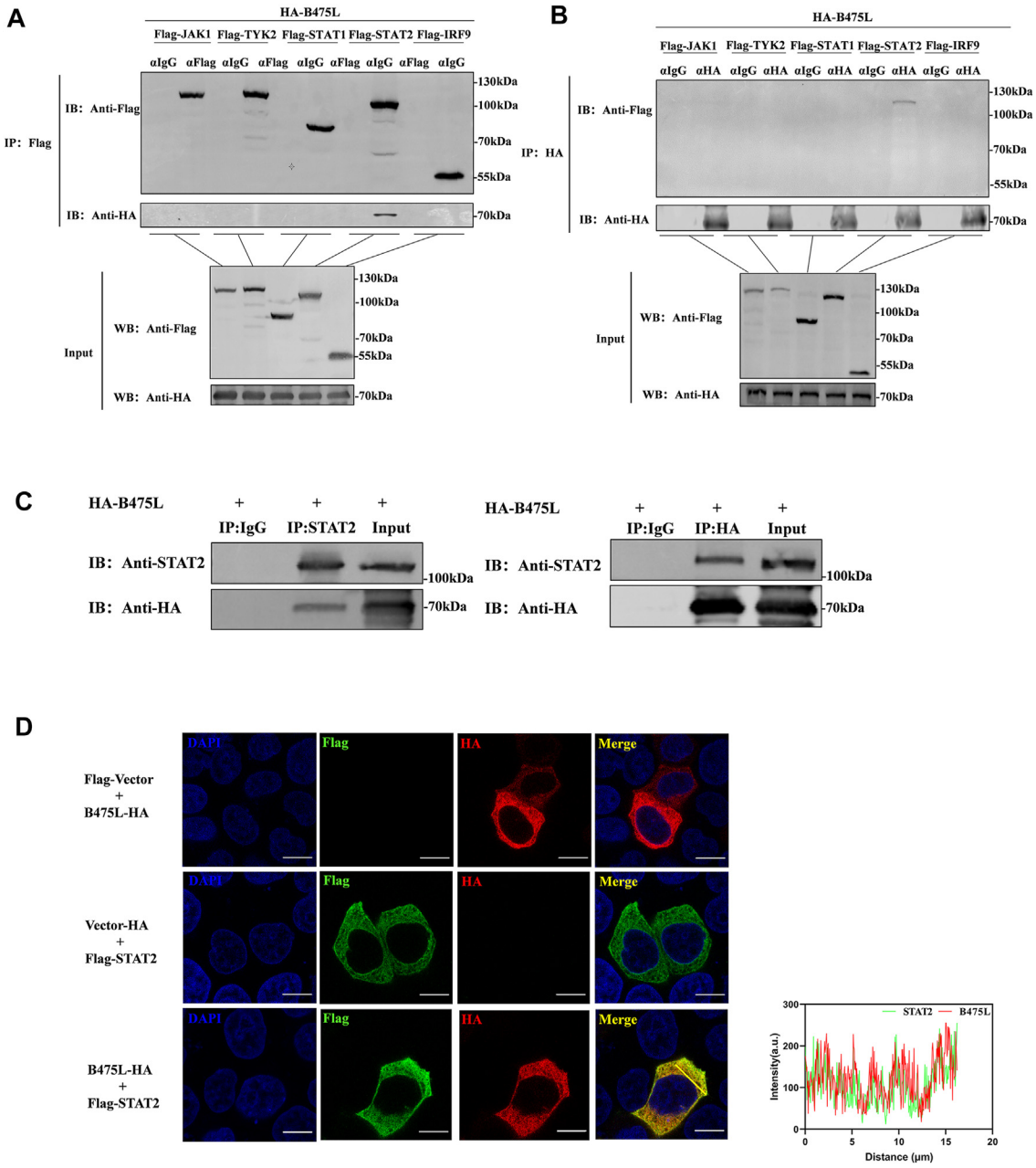


**Figure 3. ASFV pB475L interacts with STAT2.** *A* and *B*, HEK293T cells were seeded in 100-mm Petri dishes and then transfected with the pB475L expression plasmid (5000 ng/well) and JAK1 TYK2/STAT1 STAT2/IRF9 transfection (5000 ng/well). After 24 h, the cells were lysed, and HA and FLAG antibodies were used for IP and IB assays. *C*, HEK293T cells seeded in 100-mm Petri dishes were transfected with pB475L expression plasmid (10,000 ng/well) for 24 h. The cells were lysed, and HA and STAT2 antibodies were used for IP and IB assays. *D*, HeLa cells in glass-bottom dishes were cotransfected with pB475L expression plasmid (1000 ng/well) and STAT2 (1000 ng/well) for 24 h. The subcellular localization of the indicated proteins was analyzed by confocal microscopy. Nuclei were stained with DAPI. For fluorescence intensity analysis, *red and green lines* (plot, *bottom right*) indicate the fluorescence of the corresponding color. The ordinate represents the *gray value* of the fluorescence channel, and the abscissa represents the relative position of the *yellow lines* in the merged plot. Scale bar represents 10 μm. ASFV, African swine fever virus; DAPI, 4′,6-diamidino-2-phenylindole; HA, hemagglutinin; HEK293T, human embryonic kidney 293T cell line; IB, immunoblotting; IP, immunoprecipitation; IRF9, interferon regulatory factor 9; JAK, Janus-activated kinase; STAT, signal transducer and activator of transcription.

pB475L and STAT2 by confocal microscopy (Fig. 3*D*); the fluorescence intensity analysis demonstrated that pB475L and STAT2 colocalized in the cytoplasm.

### pB475L targets the C-terminal domain of STAT2 to inhibit STAT1 and STAT2 heterodimerization

Six conserved functional domains comprise STAT2: the N-terminal domains, coiled-coil domains, DNA-binding domains, linker domains, SH2D, and transcriptional activation domains (33). To explore which STAT2 domain interacts with pB475L, we generated three STAT2 truncated mutants (T1–T3; Fig. 4*A*). The co-IP assay demonstrated that pB475L interacted with STAT2-T3 (Fig. 4, *B* and *C*).

The heterodimerization of STAT1 and STAT2 proteins is essential for IFN-I signaling (34), and SH2D is a key domain for this heterodimerization. Therefore, we then investigated whether pB475L could block this heterodimerization by interacting with STAT2-T3. The co-IP assay demonstrated that pB475L inhibited the heterodimerization of STAT1 and STAT2 as well as that of p-STAT2 and p-STAT1 (Fig. 4*D*). Importantly, phosphorylation of STAT1 at Tyr701 and STAT2 at Tyr690 is critical for heterodimer formation (35), and we found that pB475L does not affect the phosphorylation at these sites (Fig. 3). Thus, we hypothesized that the competitive binding of pB475L to STAT1 and STAT2 inhibited STAT1 and STAT2 heterodimerization. IFN-II activates ISGs through STAT1 homodimerization. Therefore, we examined whether pB475L affects IFN-II-activated ISGs (36). We found that pB475L did not affect IFN-II-activated GBP1 and IRF1 (Fig. S3), demonstrating that pB475L specifically targets STAT2 to coordinate IFN-I signaling.

### pB475L inhibits the nuclear translocation of STAT1/2

We next explored the effect of pB475L on STAT1/2 nuclear translocation in IFN-I-treated cells. pB475L was transfected into HeLa cells and treated with IFN-I for 2 h, followed by an indirect immunofluorescence assay using STAT1 and STAT2 antibodies and analysis *via* confocal microscopy. As expected, nuclear translocation of STAT1 and STAT2 occurred in IFN-I-treated cells transfected with an empty vector. In contrast, STAT1 and STAT2 nuclear translocation was significantly inhibited in IFN-I-treated pB475L-expressing cells (Fig. 5*A*). To confirm that pB475L blocks STAT1/2 nuclear translocation, nuclear and cytoplasmic proteins were isolated from HeLa cells transfected with pB475L or the empty vector and treated with IFN-I. After that, STAT1, STAT2, p-STAT1, and p-STAT2 protein levels were detected in the nucleus and cytoplasm. Ectopic expression of pB475L increased the cytoplasmic STAT1/2 and p-STAT1/2 protein levels and decreased the nucleic STAT1/2 and p-STAT1/2 protein levels (Fig. 5, *B* and *C*). Therefore, pB475L inhibits IFN-I-mediated STAT1/2 nuclear translocation.

### pB475L interacts with STAT2 through multiple amino acid residues

Next, we generated three truncated mutants of pB475L (T4–T6; Fig. 6*A*) and examined their interactions with STAT2. We found that these three mutants interacted with STAT2 (Fig. 6, *B* and *C*). To identify the amino acid residues that mediate the interactions between pB475L and STAT2, we studied the protein structures of STAT2 and pB475L using the online Alphafold2 server (https://alphafold.ebi). Interactions in the STAT2–pB475L complex were analyzed by gram-x online software (http://gramm.compbio.ku.edu/). We aimed to predict the potential interaction interfaces and the responsible amino acid residues. Docking results showed that 12 pairs of amino acid residues formed hydrogen bonds at the interaction interface (Fig. 6*D*). Consistent with co-IP results, the interacting residues are dispersed in pB475L (*red markers*), whereas responsible STAT2 residues were mostly located in its C-terminal domain (*blue markers*). Next, we identified seven amino acid residues (*i.e.*, His36, Ser79, Leu82, Glu268, Gln373, Glu456, and Ser458) of pB475L that mediated its interactions with STAT2 C-terminal domain and mutated them to alanine. We found that the construct with the seven point mutations (pB475L$^{7PM}$) did not interact with STAT2 (Fig. 6*E*), indicating that these amino acid residues of pB475L are essential for interactions with STAT2.

### ASFV-B475L$^{7PM}$ construction

The ORF of the B475L gene is in the middle of the ASFV strain GZ201801 genome; the ORF is 1428 bps and encodes 475 amino acids, and its forward strand position is 98,068 to 99,495.

To evaluate pB475L conservation among different strains, we compared the pB475L aa sequences of the representative strains of ASFV genotypes I and II (Fig. S4), finding that pB475L was highly conserved in both. Next, we monitored the transcription phase of B475L in ASFV, finding that the B475L transcription level peaked at 6 to 12 h after ASFV infection (Fig. 7*A*). After that, to determine the immunosuppressive capacity of pB475L in ASFV infection, we constructed the ASFV point mutant recombinant strain inserted into the p72mCherry coding reporter cassette (Fig. 7*B*). Fluorescence microscopy indicated that we successfully rescued ASFV-B475L$^{7PM}$ (Fig. 7*C*); thus, the ASFV-B475L$^{7PM}$ was purified by the limited fold dilution method, and primers for the B475L gene were designed to detect the ASFV-B475L$^{7PM}$. The results of PCR showed that ASFV-B475L$^{7PM}$ was successfully constructed (Fig. 7*D*). From 12 h, the growth characteristics of ASFV-B475L$^{7PM}$ were slightly lower than those of ASFV-WT (Fig. 7*E*). This may be caused by the higher level of ISGs induced by ASFV-B475L$^{7PM}$.

### ASFV-B475L$^{7PM}$ attenuates IFN-I signaling inhibition

Avirulent strains lacking the IFN suppressor gene induce higher levels of ISG15 compared with ASFV-WT (37). Thus, we monitored the ISG15 and ISG54 transcription levels induced by ASFV and ASFV-B475L$^{7PM}$ in porcine alveolar macrophages (PAMs) infected at different time points. After 6 h (*i.e.*, the start of peak B475L transcription), ASFV-B475L$^{7PM}$ induced significantly higher ISG expression than ASFV-WT (Fig. 8*A*). Moreover, compared with ASFV-WT

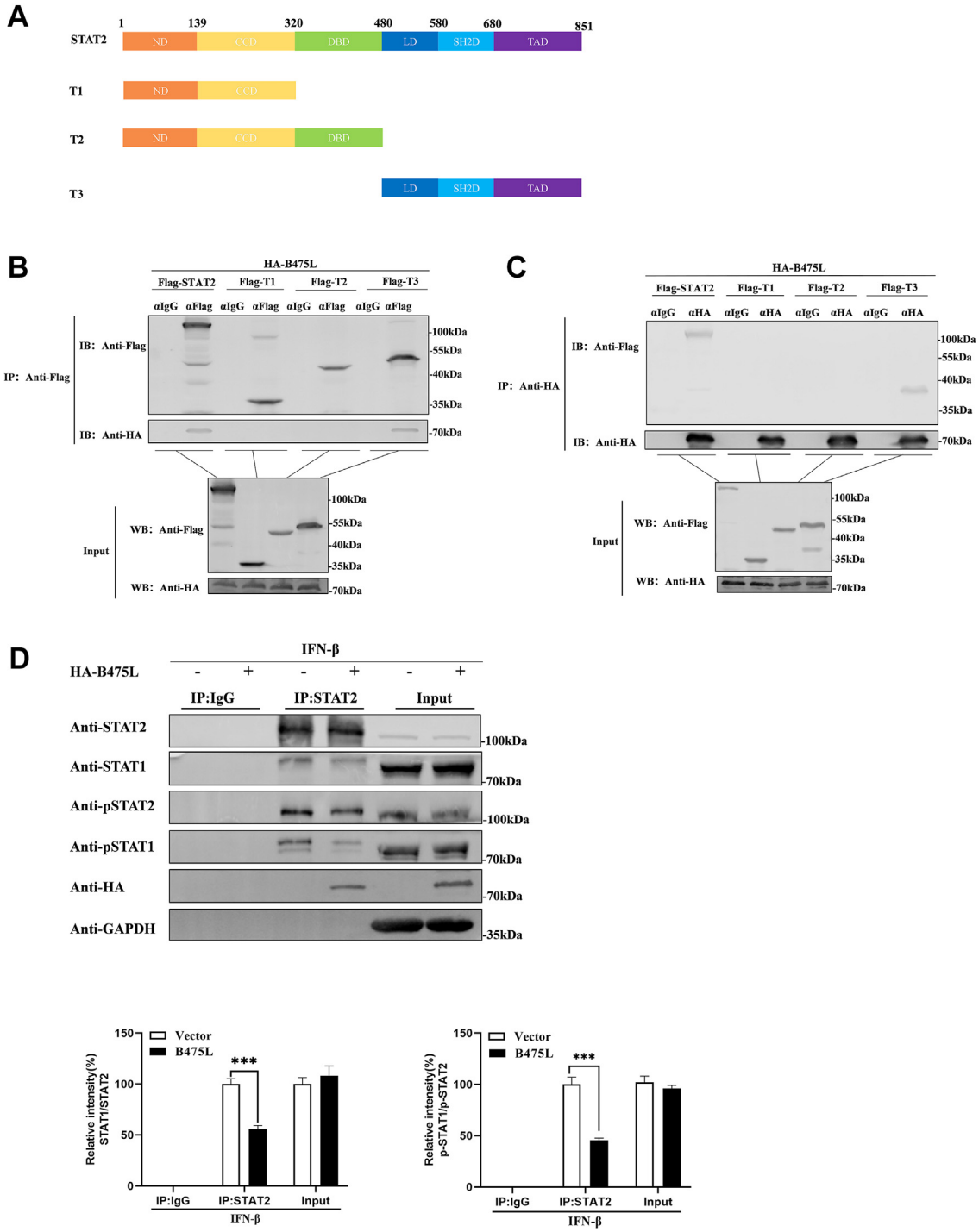


**Figure 4. pB475L interacts with the C-terminal domain of STAT2 to inhibit the heterodimerization of STAT1 with STAT2.** *A*, schematic representation of full-length STAT2 and its deletion mutants. *B* and *C*, HEK293T cells were cotransfected with pB475L expression plasmid (5000 ng/well) and the STAT2 mutants (T1/T2/T3; 5000 ng/well) in 100-mm Petri dishes. IP with the cell lysates was performed after 24 h using HA and FLAG antibodies, followed by protein IB. *D*, HEK293T cells were seeded in 100-mm Petri dishes and transfected with the pB475L expression plasmid (10,000 ng/well). After 24 h, the cells were stimulated with IFN-β (1000 U/ml) for 2 h, then the cell lysates underwent IP using STAT2, followed by IB with p-STAT1, p-STAT2, and HA. The relative WB intensity of p-STAT1 to p-STAT2 was quantified and analyzed. ***$p < 0.001$. HA, hemagglutinin; HEK293T, human embryonic kidney; IFN-β, interferon beta; IB, immunoblotting; IP, immunoprecipitation; p-STAT, phosphorylated STAT; STAT, signal transducer and activator of transcription.

infection, ASFV-B475L$^{7PM}$ infection significantly attenuated the inhibitory effect of IFN-I on ISG transcription levels after 24 h in IFN-I-treated PAMs (Fig. 8*B*). In conclusion, ASFV-B475L$^{7PM}$ induced higher levels of ISGs and attenuated the inhibitory effect on IFN-I signaling compared with ASFV-WT. However, the level of ISG induced by ASFV-B475L7PM was still low. MGF505-7R and MGF360-9L inhibit IFN-I signaling through pathways distinct from pB475L (26, 27); thus, we hypothesized that inhibition of IFN-I signaling by MGF505-7R, MGF360-9L, and pB475L could be additive. The results

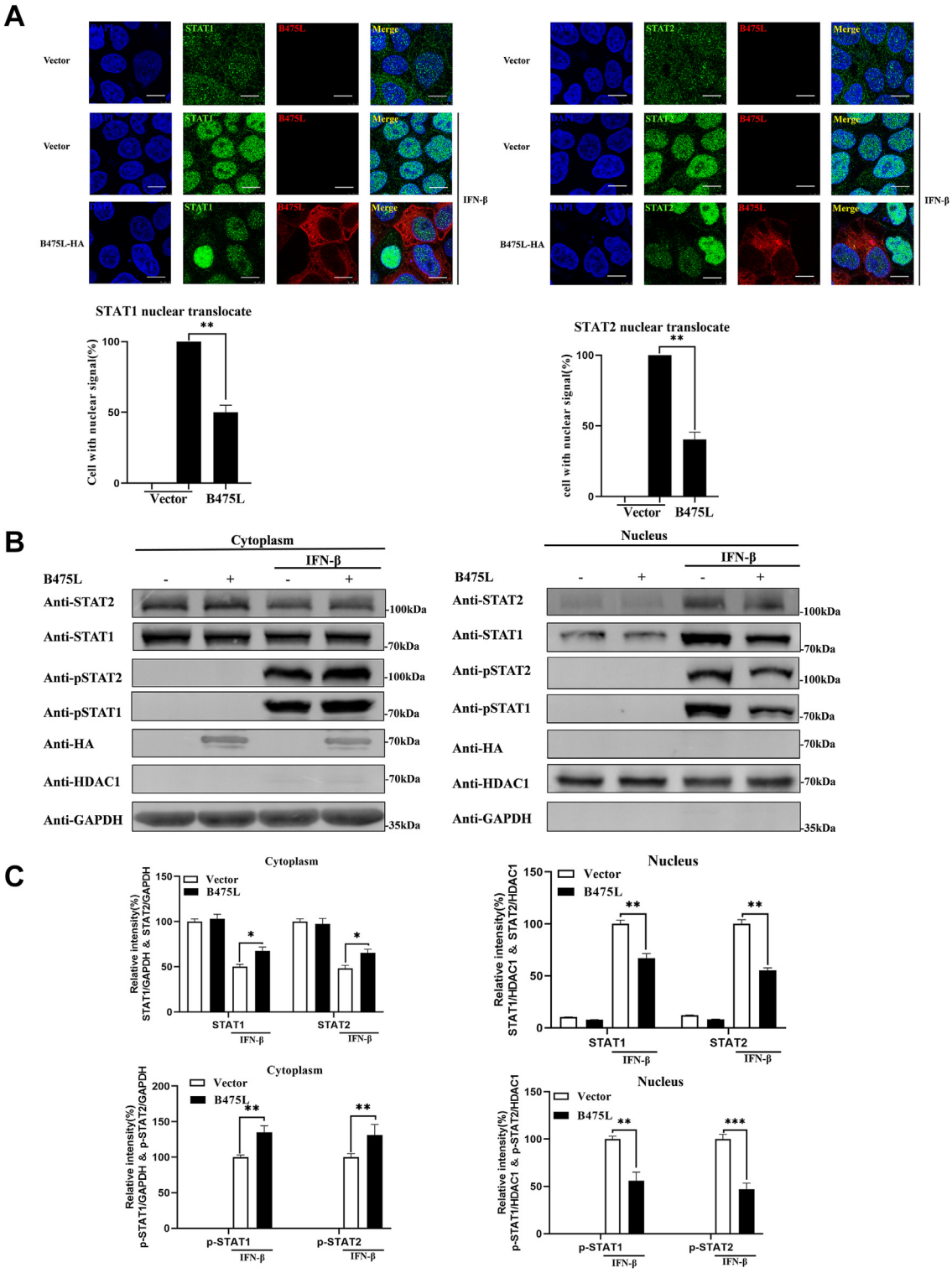


**Figure 5. pB475L inhibits STAT1/2 nuclear translocation.** *A*, HeLa cells were seeded in glass-bottom dishes and transfected with pB475L expression plasmid (2500 ng/well). After 24 h, they were stimulated with IFN-β (1000 U/ml) for 2 h, and the percentage of STAT1 and STAT2 nuclear translocation was quantified. *B*, HeLa cells were seeded in 6-well plates and transfected with pB475L expression plasmid (2500 ng/well). After 24 h, the cells were stimulated with IFN-β (1000 U/ml) for 2 h, and then cytoplasmic and nuclear proteins were extracted from the cells using NE-PER Nuclear and Cytoplasmic Extraction Kit. P-STAT1 and p-STAT2 in the nucleus and cytoplasm were detected by Western blot. GAPDH and heat shock protein HDAC1 were used as cytoplasmic and nuclear markers, respectively. *C*, the relative intensities of p-STAT1 and p-STAT2 Western blots were quantified using GAPDH and HDAC1 proteins as the reference for cytoplasmic and nuclear proteins, respectively. $^{**}p < 0.01$; $^{***}p < 0.001$. Scale bar represents 10 μm. IFN-β, interferon beta; p-STAT, phosphorylated STAT; STAT, signal transducer and activator of transcription.

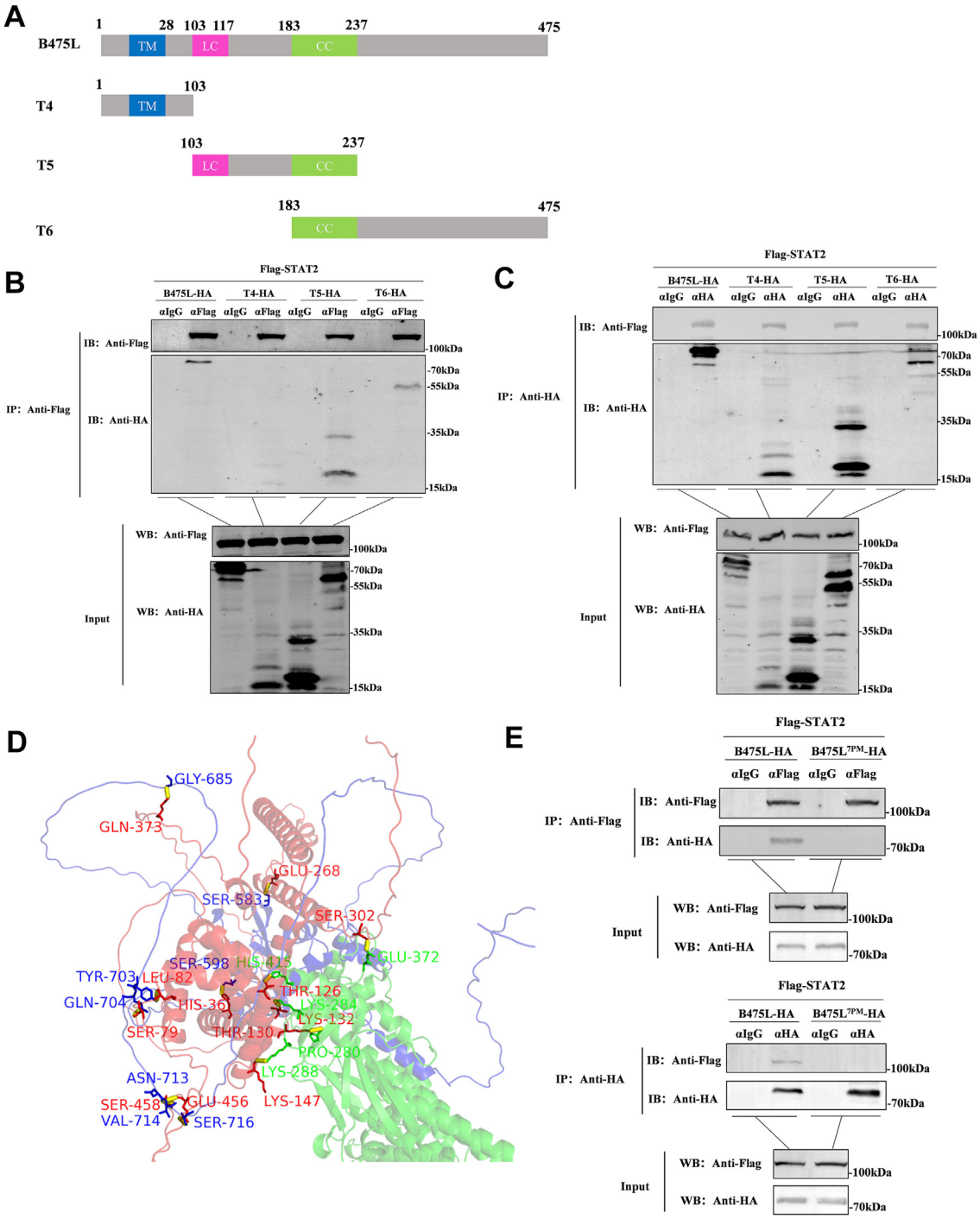


**Figure 6. Identification of B475L interacting amino acid residues with STAT2.** *A*, schematic representation of full-length B475L and its deletion mutants. *B* and *C*, HEK293T cells were cotransfected with STAT2 expression plasmid (5000 ng/well) and the pB475L mutants (T4/T5/T6; 5000 ng/well) in 100-mm Petri dishes. IP with the cell lysates was performed after 24 h using HA and FLAG antibodies, followed by protein IB. *D*, AlphaFold2 and GRAMM online servers were used to obtain the prediction model of STAT2–pB475L interaction complex. *E*, HEK293T cells were cotransfected with STAT2 expression plasmid (5000 ng/well) and the pB475L or pB475L$^{7PM}$ (5000 ng/well) in 100-mm Petri dishes. IP with the cell lysates was performed after 24 h using HA and FLAG antibodies, followed by protein IB. HA, hemagglutinin; HEK293T, human embryonic kidney 293T cell line; IB, immunoblotting; IP, immunoprecipitation; STAT, signal transducer and activator of transcription.

of dual luciferase reporter gene showed that cotransfection of pMGF505-7R and pMGF360-9L enhanced inhibition of IFN-I signaling by pB475L (Fig. 8*C*). We suggest that expression of different proteins after infection acts as a backup mechanism to antagonize IFN-I signaling.

### *ASFV-B475L$^{7PM}$ restored the heterodimerization and nuclear translocation of STAT1 and STAT2*

Next, we aimed to determine the molecular mechanisms underlying the immune function of pB475L in ASFV-infected PAMs and to compare the effects of ASFV-WT and ASFV-

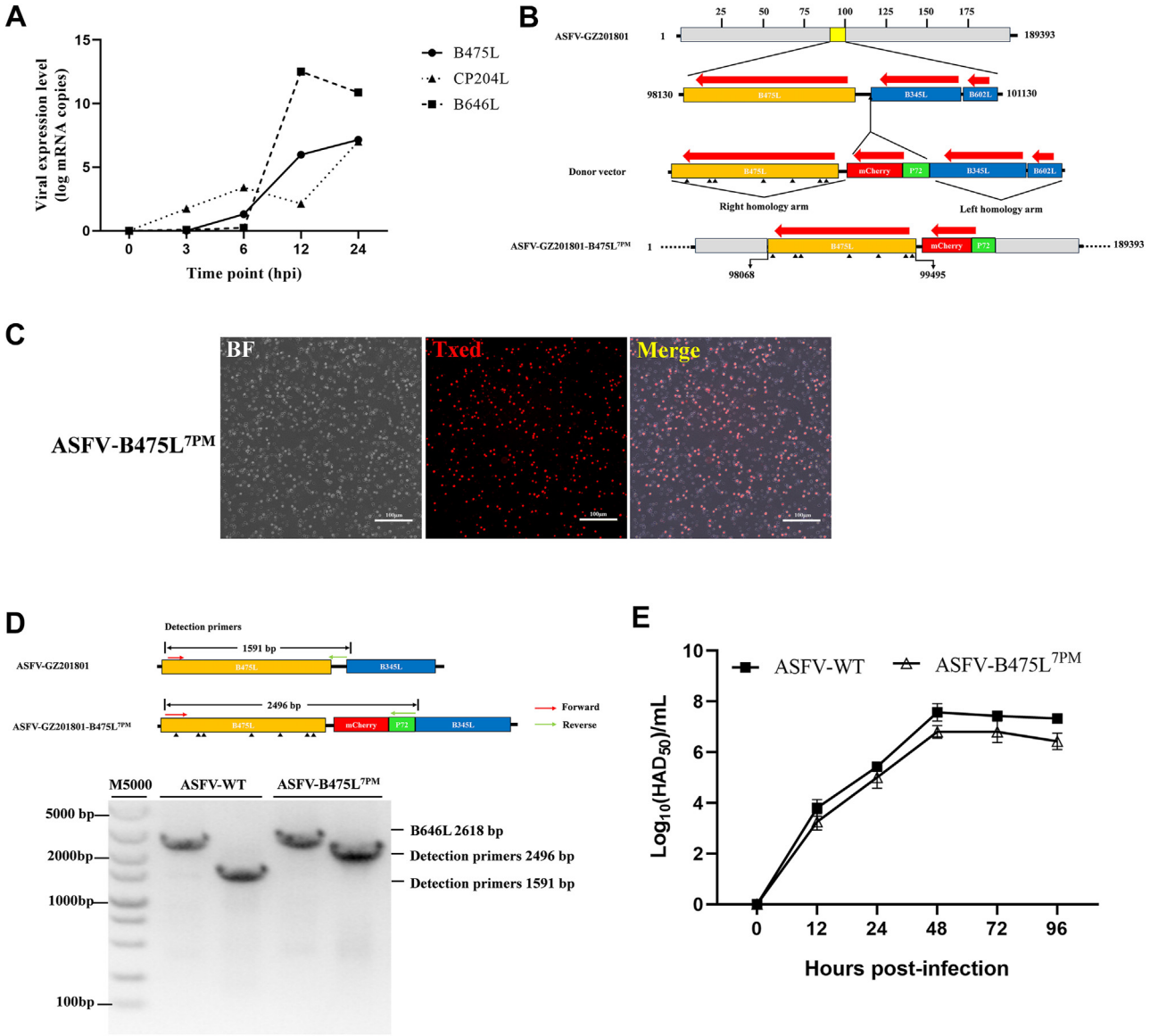


**Figure 7. The construction of ASFV-B475L$^{7PM}$.** *A*, PAMs were infected with ASFV (multiplicity of infection [MOI] = 0.1), and cells were collected at the indicated time points after infection. Quantitative PCR was used to detect the mRNA expression levels of B475L, CP204L, and B646L. Porcine GAPDH was used as an internal loading control. The transcription phase of B475L was monitored. *B*, the ASFV–B475L$^{7PM}$ construction strategy by homologous recombination. The *black triangles* indicate the introduced point mutations. *C*, after multiple rounds of limited-fold dilution, the labeled recombinant strains were observed under a fluorescence microscope. *D*, schematic design of primers for detection of recombinant strains. The recombinant strains were identified by PCR. Viral DNA obtained from the parental ASFV or ASFV-B475L$^{7PM}$ mutant was amplified by PCR using B475L and B646L primers (B646L primer was used as an indicator of genomic input). *E*, PAMs were infected with ASFV-WT (MOI = 0.01) or ASFV-B475L$^{7PM}$ (MOI = 0.01), and the virus titer was detected by the HAD50 (50% hemadsorption dose) method at the specified time points after infection, and growth curves were created. ASFV, African swine fever virus; PAM, porcine alveolar macrophage.

B475L$^{7PM}$ on STAT1/2 heterodimerization using co-IP and protein quantification assays. The STAT1 level precipitated by STAT2 was significantly lower in the ASFV-WT group than in the mock group. However, the STAT1 level was significantly higher in the ASFV-B475L$^{7PM}$ group than in the ASFV-WT group (Fig. 9*A*).

To determine whether ASFV-B475L$^{7PM}$ restores STAT1/2 nuclear translocation, we isolated nuclear and cytoplasmic proteins from PAMs infected with ASFV-WT or ASFV-B475L$^{7PM}$ strains, then used p-STAT1 and p-STAT2 antibodies to detect protein levels in the nucleus and cytoplasm (Fig. 9, *B* and *C*). As expected, ASFV-WT significantly inhibited the nuclear translocation of p-STAT1/2, but p-STAT1/2 accumulation was not observed in the cytoplasm, possibly because of the inhibition of STAT1/2 phosphorylation by ASFV (38). Furthermore, p-STAT1/2 expression was significantly higher in PAMs infected with ASFV-B475L$^{7PM}$ than in those infected with ASFV-WT. Next, we infected PAMs with ASFV-WT or ASFV-B475L$^{7PM}$ and observed the nuclear translocation of STAT1 and STAT2 by confocal microscopy. As shown in Figure 9*D*, consistent with the WB results, PAMs infected with ASFV-B475L$^{7PM}$ showed more STAT1/2 nuclear localization (position marked by *white arrow*) compared with PAMs infected with ASFV-WT. In brief,

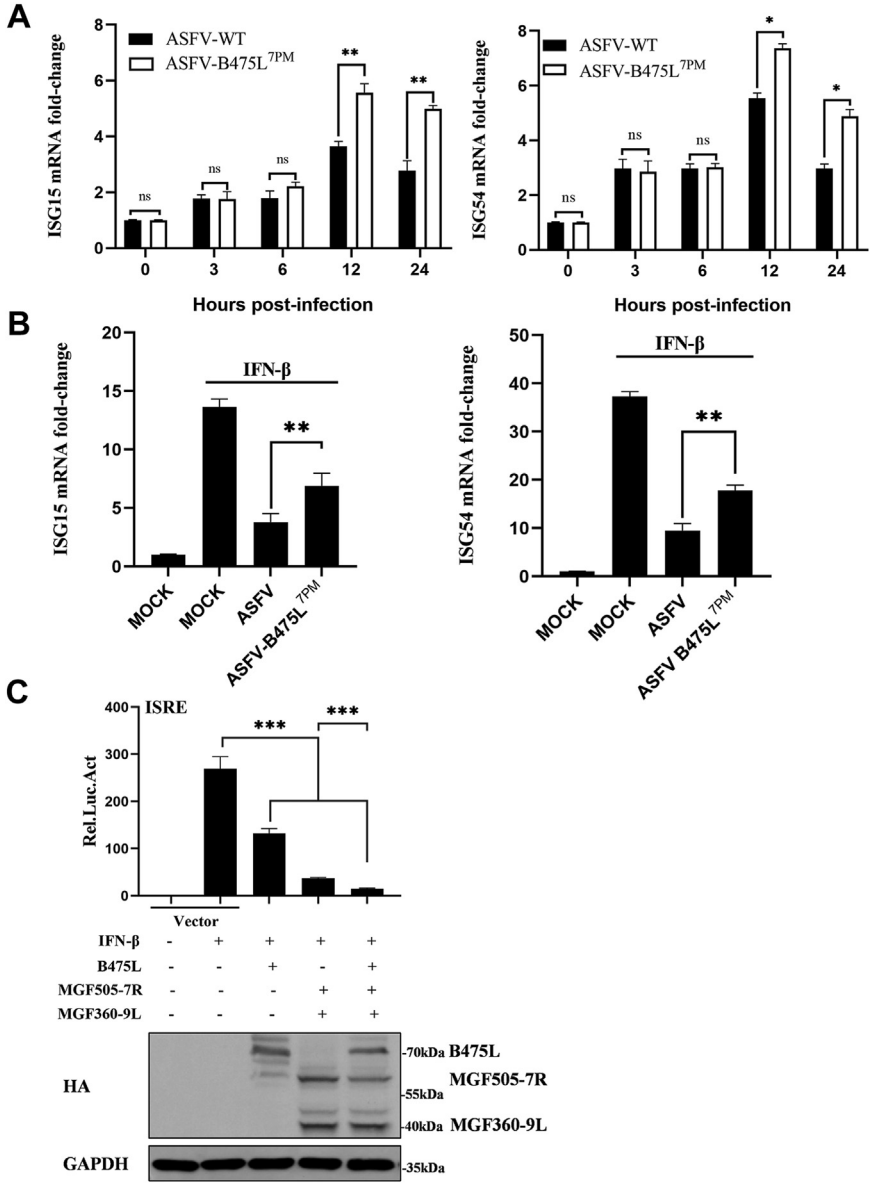


**Figure 8. Effects of ASFV-WT and ASFV-B475L$^{7PM}$ on IFN-I signaling.** *A*, PAMs were infected with ASFV-WT or ASFV-B475L$^{7PM}$ (multiplicity of infection [MOI] = 1), and the cells were harvested at the indicated time points for detecting ISG15 and ISG54 mRNA expression. *B*, PAMs were infected with ASFV-WT (MOI = 1) or ASFV-B475L$^{7PM}$ (MOI = 1) for 24 h and then treated with IFN-β (1000 U/ml) for 8 h. The ISG15 and ISG54 mRNA levels were detected by reverse transcription-quantitative PCR. *C*, HEK293T cells cultured in 24-well plates were transfected with ASFV B475L or MGF505-7R and MGF360-9L expression plasmid or empty vector (200 ng/well), pRL-TK (25 ng/well), and ISRE Luc (125 ng/well). After 24 h, the cells were treated with 1000 U/ml IFN-β for 8 h and analyzed by dual luciferase reporter. $^{**}p < 0.01$; $^{***}p < 0.001$. ASFV, African swine fever virus; HEK293T, human embryonic kidney 293T cell line; IFN-I, type I interferon; IFN-β, interferon beta; ISG, interferon-stimulated gene; PAM, porcine alveolar macrophage.

ASFV-B475L$^{7PM}$ resumed STAT1–STAT2 heterodimerization and nuclear translocation.

## Discussion

As the first line of innate immunity, IFN-I plays an important role against viruses (30). Highly pathogenic ASFV has evolved various immune evade strategies to suppress the host's IFN response, and several of these proteins have been reported to disrupt host innate immunity by inhibiting IFN-I signaling. For instance, pMGF360-9L inhibits IFN-I signaling by degrading STAT1 and STAT2 through apoptotic and proteasomal pathways (26). pI215L also inhibits IFN-I signaling by degrading IRF9 through the autophagic pathway (39) However, several ASFV proteins with unknown functions exist, and the potential mechanisms by which ASFV inhibits IFN-I signaling still need to be explored.

ASFV pB475L is a nonstructural protein with a previously unknown function (40). Here, we report for the first time that it elicits immunosuppressive effects. Ectopic expression of pB475L inhibited IFN-I-activated ISRE promoter activity and ISG transcription. Surprisingly, pB475L did not affect the expression or phosphorylation of individual proteins in the IFN-I signaling pathway, suggesting that pB475L mainly targeted downstream signal transduction. Notably, we found an interaction between pB475L and STAT2 protein. STAT2 is a

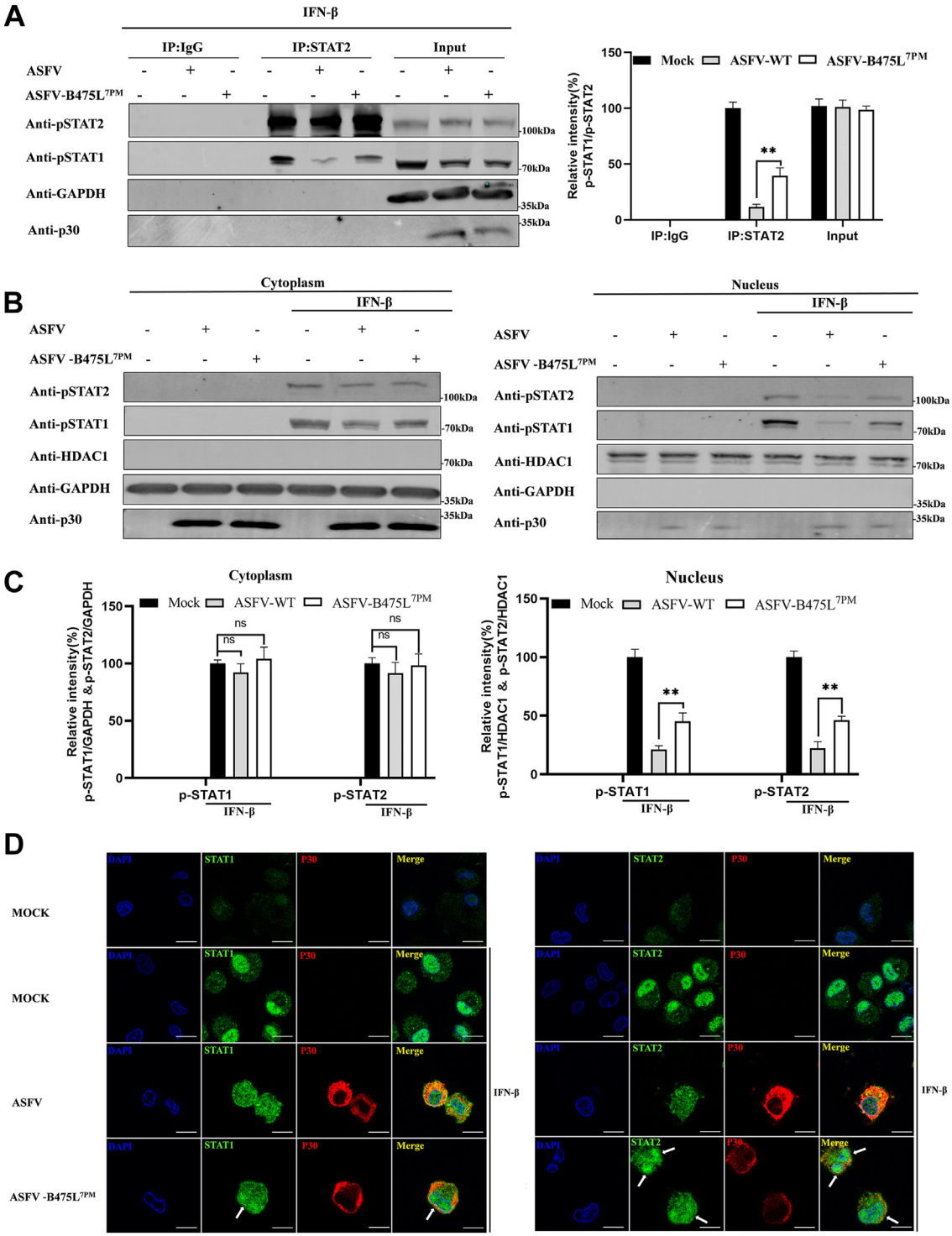


**Figure 9. Effects of ASFV-WT and ASFV-B475L$^{7PM}$ on heterodimerization and nuclear translocation of STAT1 and STAT2.** *A*, PAMs were infected with ASFV-WT or ASFV-B475L$^{7PM}$ (MOI = 0.5) for 24 h, followed by IFN-β stimulation for 2 h. Cell lysates were coimmunoprecipitated using STAT2 antibody, and p-STAT1 and p-STAT2 antibodies were used for protein immunoblot. Relative intensities of the precipitated p-STAT1 protein blots were quantified using p-STAT2 protein as a reference. *B*, PAMs were infected with ASFV-WT or ASFV-B475L$^{7PM}$ (multiplicity of infection [MOI] = 0.5) for 24 h, followed by IFN-β stimulation for 2 h. p-STAT1 and p-STAT2 in nuclear and cytoplasmic compartments were detected by Western blot. GAPDH and heat shock protein HDAC1 were used as cytoplasmic and nuclear markers, respectively. *C*, the relative intensities of p-STAT1 and p-STAT2 Western blots were quantified using GAPDH and HDAC1 proteins as the reference for cytoplasmic and nuclear proteins, respectively. $^{**}p < 0.01$. *D*, PAMs were infected with ASFV-WT or ASFV-B475L$^{7PM}$ (MOI = 0.5) for 24 h, followed by IFN-β stimulation for 2 h. The nuclear translocation of STAT1/2 was observed by confocal microscopy. Scale bar represents 10 μm. ASFV, African swine fever virus; IFN-β, interferon beta; PAM, porcine alveolar macrophage; p-STAT, phosphorylated STAT; STAT, signal transducer and activator of transcription.

key transcription factor in the JAK–STAT signaling pathway (41) with six conserved structures. Among them, SH2D comprises a β-sheet surrounded by two α helices, and the tyrosine residue Tyr690 of STAT2 is directly adjacent to SH2D (16, 42). Phosphorylation of SH2D, STAT1 tyrosine residue Tyr702, and STAT2 tyrosine residue Tyr690 plays important roles in STAT1 and STAT2 heterodimerization (10, 34).

Blocking immunosuppression by severing the interaction between proteins in the host immune signaling pathway is a common viral immune evade strategy. For example, ASFV pMGF505-7R interacts with IRF9 to inhibit ISGF3 trimeric and IFN-I signaling (27). The Ebola virus VP24 protein binds karyopherin subunit alpha 1, disrupting the formation of the pSTAT1–karyopherin subunit alpha 1 complex and hindering STAT1 nuclear transport (43). Bacteria have a similar function, and *Staphylococcus aureus* inhibits STAT1 and STAT2 heterodimerization to promote influenza virus infection (44). In this study, we found that pB475L inhibited IFN-I-mediated p-STAT1/2 heterodimerization by interacting with the C-terminal domain of STAT2. Importantly, pB475L did not inhibit the phosphorylation of STAT1 at Tyr701 or STAT2 at Tyr690. We, therefore, reasoned that pB475L inhibited STAT1 and STAT2 heterodimerization by competing with the C-terminal domain for STAT2 binding. Homodimerization and heterodimerization mediated by their tyrosine phosphorylation triggers STAT1 and STAT2 nuclear translocation (20). Thus, as expected, pB475L inhibited IFN-I-mediated nuclear translocation of STAT1 and STAT2.

Notably, our constructed recombinant ASFV-B475L$^{7PM}$ strain attenuated IFN-I inhibition and induced higher levels of ISGs compared with ASFV-WT. ASFV-B475L$^{7PM}$ showed similar potential to other ASFV gene deletion attenuated strains. A137R targets TANK-binding kinase 1 and antagonizes IFN-I production, whereas ASFVΔA137R induces higher levels of IFN-I in PAMs (45). MGF505-7R, the primary ASFV virulence gene, inhibits multiple nodes in the upstream and downstream IFN-I pathways; thus, recombinant ASFVΔMGF505-7R induces higher levels of IFN-I and ISGs in PAMs (22, 27, 46). In this study, we found abundant B475L transcription 6 to 12 h after infection. Moreover, ASFV-B475L$^{7PM}$ induced higher levels of ISGs after 12 and 24 h but not after 3 and 6 h, compared with ASFV-WT. These results highlight the function of pB475L during ASFV. ASFV-B475L$^{7PM}$ significantly restored STAT1 and STAT2 heterodimerization and, thus, nuclear translocation in IFN-I-treated PAMs. However, as expected, it did not fully restore STAT1 and STAT2 nuclear translocation, owing to other proteins that can inhibit IFN-I signaling in various ways (26, 27, 39, 47). In addition, ASFV still has several proteins with unknown functions.

This study reports a novel ASFV immune evade mechanism and clarifies the immunosuppressive function of ASFV pB475L, enriching our overall understanding of ASFV immune evade and the pB475L regulation in host innate immunity (Fig. 10).

## Experimental procedures

### *Cells and viruses*

HEK293T and HeLa cells were preserved by the Department of Infectious Diseases, South China Agricultural University. PAMs were obtained from 4-week-old specific pathogen-free pigs. HEK293T and HeLa were cultured in Dulbecco's modified Eagle's medium (Gibco/Thermo Fisher Scientific) medium containing 10% fetal bovine serum (Gibco) and 1% penicillin, streptomycin, and amphotericin B. PAMs were cultured in 1640 (Gibco) medium supplemented with 10% fetal bovine serum and 1% penicillin, streptomycin, and amphotericin B. All cells were cultured at 37 °C and 5% $CO_2$.

The ASFV-GZ201801 strain was provided by the College of Veterinary Medicine, South China Agricultural University, and ASFVΔB457L was a recombinant strain constructed from the parent GZ2018101 strain. All procedures involving live ASFV were performed in the BSL-3 laboratory of the College of Veterinary Medicine, South China Agricultural University.

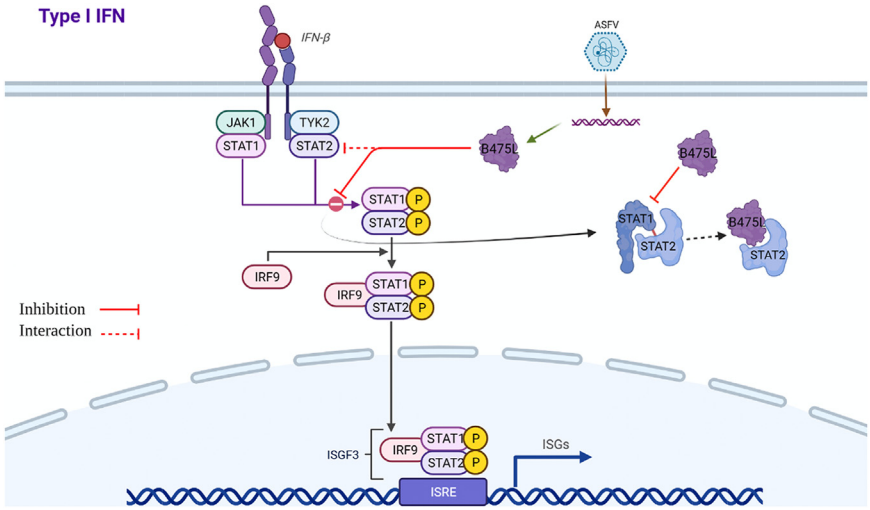


**Figure 10. Schematic diagram of the antagonism of IFN-I signaling by ASFV pB475L.** ASFV pB475L negatively regulates IFN-I signaling by interacting with STAT2 and inhibiting the heterodimerization between STAT1 and STAT2, thereby inhibiting the nuclear translocation of STAT1 and STAT2. ASFV, African swine fever virus; IFN-I, type I interferon; STAT, signal transducer and activator of transcription.

### Antibodies and reagents

The following murine monoclonal antibodies were used: P30 (CP204L) was prepared and supplied by our laboratory; HA (M20003) and FLAG (M20008) (Abmart); histone deacetylase 1 (*i.e.*, HDAC1; Santa Cruz Biotechnology); and GAPDH (HC301-01; TransGen Biotech). The following rabbit monoclonal antibodies were used: p-Jak1 (catalog no.: 74129), p-Tyk2 (68790), HA (3724), p-STAT1 (9167), p-STAT2 (88410) (Cell Signaling Technology). The following rabbit polyclonal antibodies were used: STAT2 (16674-1-AP), STAT1 (10144-2-AP), STAT2 (16674-1-AP), STAT1 (10144-2-AP), and IRF9 (14167-1-AP) (Proteintech). IRDye 800CW Goat (polyclonal) Anti-Rabbit/Mouse immunoglobuolin G (IgG) (H + L) was purchased from LI-COR. Goat anti-Rabbit/Mouse IgG (H + L) Cross-Adsorbed Secondary Antibody Alexa Fluor 488/555/647 was purchased from Thermo Fisher Scientific.

Murine IgG (A7031) and rabbit IgG (A7016) were purchased from Beyotime, Inc. Protein A/G Agarose (sc-2003) was purchased from Santa Cruz Biotechnology. Lipofectamine 3000 transfection reagent (L3000150) and the NE-PER Nuclear and Cytoplasmic Extraction Kit were purchased from Thermo Fisher Scientific. TransIT-LT1 Transfection Reagent (MIR 2300) was purchased from Mirus Bio, and the Cell Counting Kit-8 assay was purchased from Beyotime, Inc.

### Plasmids

Luciferase reporter plasmid ISRE Luc, pRL-TK, and PCDNA3.1-FLAG-JAK1/TYK2/STAT1/STAT2/IRF9 were preserved in our laboratory. The ASFV GZ201801 B475L coding sequence was cloned into a mammalian expression vector containing HA-label pCAGGS at the carboxyl terminal using the EcoRI and KpnI cleavage sites. Using amplified complementary DNA (cDNA) sequences of PK-15 cells, STAT2-truncated mutants (STAT1-T1, STAT2-T2, and STAT2-T3) were cloned into PCDNA3.1-FLAG mammalian expression vectors. Using amplified cDNA sequences of ASFV, B475L-truncated mutants (B475L-T4, B475L-T5, and B475L-T6) were cloned into PCAGGS-HA mammalian expression vectors. B475L$^{7PM}$ was synthesized by Beijing Tsingke Biotech and cloned in PCAGGS-HA vector.

The recombinant ASFV gene was constructed by using the ASFV genome and B475L$^{7PM}$ plasmid as the template, with 1500 bp of the left and 1508 bp of the right homology arms of the donor plasmid and the P72 promoter. The p72 promoter and mCherry were added in the middle of the left and right homology arms and successfully cloned into the pBSK plasmid by homologous recombination. The primers used in this experiment are listed in Table S1.

### Luciferase assay

HEK293T cells were transiently transfected with pGL3-ISRE-Luc, pRL-TK luciferase vector, and the indicated plasmids. After 24 h, the cells were stimulated with universal IFN-β (1000 U/ml) for 8 h. Luciferase activity was measured using a dual luciferase assay system (Promega following the manufacturer's instructions.

### WB and IP

HEK293T cells or PAM cells were directly lysed 24 h after transfection/infection or stimulated with universal IFN-β (1000 U/ml) for 2 h before lysing. The cells were lysed in NP-40 protein lysate supplemented with 1% PMSF (Beyotime, Inc), then 5× protein sample buffer (Beyotime, Inc) or 5× native sample buffer (Sangon Biotech, Inc) was added to the sample, and boiled for 8 min. For the WB analysis, the protein sample was run on a 10% sodium dodecyl-sulfate polyacrylamide gel electrophoresis gel and transferred to a polyvinylidene difluoride membrane (Beyotime, Inc). The membrane was incubated in 5% skim milk powder dissolved in 0.5% TSUM 20 Tris-buffered saline with Tween-20. After the membrane was incubated with the relevant primary antibody (mixed with 2% bovine serum albumin in Tris-buffered saline with Tween-20), followed by the secondary antibody (IRDye 800CW Goat [polyclonal] Anti-Rabbit/Mouse IgG [H + L]; 1:15,000 dilution).

For co-IP, HEK293T cells or PAM cells were inoculated in a 10-mm cell culture dish and transfected with a specified plasmid or infected with a specified virus. The cells were lysed in the cell lysis buffer for WB and IP (Beyotime, Inc) 24 h after transfection/infection. After that, the coupled IP antibody Protein A/G was incubated with the protein lysate at 4 °C for 2 to 4 h and then washed three times with phosphate-buffered saline with Tween 20. Finally, sodium dodecyl-sulfate protein loading buffer was added, the sample was boiled for 8 min, and then sodium dodecyl-sulfate polyacrylamide gel electrophoresis and WB were performed.

### Confocal microscopy

HeLa cells were inoculated into 24-well glass bottom plates for transfection with the relevant plasmids. Twenty-four hours after transfection, the cells were stimulated with universal IFN-β (1000 U/ml) for 2 h or left unstimulated. After that, they were then fixed with 4% paraformaldehyde for 10 min and permeabilized with PBS containing 0.3% Triton X-100. After three washes with PBS, the cells were incubated with 2% bovine serum albumin at 37 °C for 1 h and then incubated with anti-STAT1 and anti-STAT2 antibodies (1:200 or 1:50 dilution) as well as anti-P30, anti-HA, and anti-FLAG antibodies (1:1000 dilution). Samples were incubated with primary antibody overnight at 4 °C and secondary antibody (Alexa Fluor 488/555/647) for 1 h at room temperature. After that, 4′,6-diamidino-2-phenylindole (Beyotime, Inc) was used to stain the cells for 15 min, and fluorescence images were acquired using a confocal laser scanning microscope (Leica TCS SP8).

### RNA extraction and real-time quantitative PCR

Total RNA was extracted with Trizol reagent (Invitrogen/Thermo Fisher Scientific), and RNA was reverse transcribed using reverse transcriptase (Vazyme-RL201; Vazyme Biotech). The transcribed cDNA was used for quantitative PCR using AceQ quantitative PCR SYBR Green Master Mix (Vazyme-Q121; CFX96 PCR Detection System; Bio-Rad). The abundance of individual mRNA transcripts in each sample was

determined three times, and the expression levels were normalized to GAPDH or actin. The quantitative PCR primers are shown in Table S2.

### Construction of the ASFV gene deletion strain

ASFV-B475L$^{7PM}$ was constructed by homologous recombination using ASFV GZ201801 as the backbone. The ASFV p72 promoter fragment, mCherry fragment, and 1.5-kb upstream and downstream sequences of B475L were cloned into a pBSK vector by homologous recombination. After that, the ASFV-B475L$^{7PM}$ homologous arm donor plasmid screening expression cassette, the PBSK-B475L-mCherry construct, and the plasmid were transfected into PAMs with TransIT-LT1 Transfection Reagent (2300; Mirus Bio). Four hours later, the PAMs were inoculated with ASFV GZ201801. Red fluorescence was observed 2 days later to collect the rescued virus. The virus was purified by limited-fold dilution.

### Viral titers

ASFV-WT or ASFV-B475L$^{7PM}$ samples were assessed by 50% hemadsorption dose assay (48). The PAMs were spread onto a 96-well plate, and the samples were diluted to a concentration of 10-1 to 10-8 by multiple dilutions and inoculated into 96-well plates. The adsorption of erythrocytes was observed for 5 days, and the 50% hemadsorption dose was calculated following the Reed–Muench method.

### Cytotoxicity assay

The Cell Counting Kit-8 assay was used to determine the cytotoxicity of transfection with different doses of B475L expression plasmid. In brief, HEK293T cells were seeded into 96-well plates and transfected with empty or B475L vectors. Experiments were performed in triplicate and included a blank control. The cells were incubated for 24 h, and then Cell Counting Kit-8 solution was added for 1 h. Finally, the absorbance was measured at 450 nm. Cytotoxicity was calculated as 1-(transfection sample absorbance/blank absorbance).

### Statistical analyses

All data represent at least two independent experiments wherein measurements were performed in triplicate. Data were analyzed by two-tailed Student's *t* test using GraphPad Prism, version 8. $p$ Values of $<0.05$ were considered statistically significant.

## Data availability

All data included in this study are available from the corresponding author upon request.

*Supporting information*—This article contains supporting information.

*Acknowledgments*—This research was funded by the National Key Research and Development Program of China (grant no.: 2021YFD1800100), The 16th Batch of Special Grants (Center) from China Postdoctoral Science Foundation (grant no.: 2023T160232), The 74th batch of China Postdoctoral Foundation General Support (grant no.: 2023M741220), Guangzhou Basic and Applied Basic Research Foundation (grant no.: 202201010490), the Research Project of Maoming Laboratory (grant no.: 2021TDQD002), and the China Agriculture Research System of MOF and MARA (grant no.: CARS-35).

*Author contributions*—Z. H. and Z. M. conceptualization; Z. H., J. Y., S. L., and C. G. formal analysis; C. K., Q. X., and H. W. investigation; C. K. data curation; Z. H., W. Z., and X. C. writing–original draft; Z. H. and S. T writing–review & editing; Z. H. and Z. M. visualization; Z. H., P. Z., L. G., and G. Z. funding acquisition.

*Conflict of interest*—The research was conducted without commercial or financial relationships that could be construed as a potential conflict of interest. The authors declare that they have no conflicts of interest with the contents of this article.

*Abbreviations*—The abbreviations used are: ASFV, African swine fever virus; cDNA, complementary DNA; Co-IP, coimmunoprecipitation; HA, hemagglutinin; HEK293T, human embryonic kidney 293T cell line; IFN-I, type I interferon; IFNAR, interferon-α/β receptor; IgG, immunoglobuolin G; IRF9, interferon regulatory factor 9; ISG, interferon-stimulated gene; ISRE, interferon-sensitive response element; JAK, Janus-activated kinase; PAM, porcine alveolar macrophage; SH2D, Src homology 2 domain; STAT, signal transducer and activator of transcription; TYK2, tyrosine kinase 2.

## References

1. Ankhanbaatar, U., Auer, A., Ulziibat, G., Settypalli, T. B. K., Gombo-Ochir, D., Basan, G., *et al.* (2023) Comparison of the whole-genome sequence of the African swine fever virus from a Mongolian wild boar with genotype II viruses from Asia and Europe. *Pathogens* **12**, 1143
2. Wang, N., Zhao, D., Wang, J., Zhang, Y., Wang, M., Gao, Y., *et al.* (2019) Architecture of African swine fever virus and implications for viral assembly. *Science* **366**, 640–644
3. Sun, E., Huang, L., Zhang, X., Zhang, J., Shen, D., Zhang, Z., *et al.* (2021) Genotype I African swine fever viruses emerged in domestic pigs in China and caused chronic infection. *Emerg. Microbes Infect.* **10**, 2183–2193
4. Muangkram, Y., Sukmak, M., and Wajjwalku, W. (2015) Phylogeographic analysis of African swine fever virus based on the p72 gene sequence. *Genet. Mol. Res.* **14**, 4566–4574
5. Njau, E. P., Machuka, E. M., Cleaveland, S., Shirima, G. M., Kusiluka, L. J., Okoth, E. A., *et al.* (2021) African swine fever virus (ASFV): biology, genomics and genotypes circulating in sub-saharan Africa. *Viruses* **13**, 2285
6. Abkallo, H. M., Hemmink, J. D., Oduor, B., Khazalwa, E. M., Svitek, N., Assad-Garcia, N., *et al.* (2022) Co-deletion of A238L and EP402R genes from a genotype IX African swine fever virus results in partial attenuation and protection in swine. *Viruses* **14**, 2024
7. Spinard, E., Rai, A., Osei-Bonsu, J., O'Donnell, V., Ababio, P. T., Tawiah-Yingar, D., *et al.* (2023) The 2022 outbreaks of African swine fever virus demonstrate the first report of genotype II in Ghana. *Viruses* **15**, 1722
8. Le, V. P., Ahn, M.-J., Kim, J.-S., Jung, M.-C., Yoon, S.-W., Trinh, T. B. N., *et al.* (2023) A whole-genome analysis of the African swine fever virus that circulated during the first outbreak in Vietnam in 2019 and subsequently in 2022. *Viruses* **15**, 1945
9. Martínez Avilés, M., Bosch, J., Ivorra, B., Ramos, Á. M., Ito, S., Barasona, J.Á., *et al.* (2023) Epidemiological impacts of attenuated African swine fever virus circulating in wild boar populations. *Res. Vet. Sci.* **162**, 104964
10. Huang, Z., Gong, L., Zheng, Z., Gao, Q., Chen, X., Chen, Y., *et al.* (2021) GS-441524 inhibits African swine fever virus infection *in vitro*. *Antivir. Res* **191**, 105081

11. Zhao, D., Sun, E., Huang, L., Ding, L., Zhu, Y., Zhang, J., *et al.* (2023) Highly lethal genotype I and II recombinant African swine fever viruses detected in pigs. *Nat. Commun.* **14**, 3096
12. Akira, S., Uematsu, S., and Takeuchi, O. (2006) Pathogen recognition and innate immunity. *Cell* **124**, 783–801
13. MacMicking, J. D. (2012) Interferon-inducible effector mechanisms in cell-autonomous immunity. *Nat. Rev. Immunol.* **12**, 367–382
14. Zanin, N., Viaris de Lesegno, C., Lamaze, C., and Blouin, C. M. (2020) Interferon receptor trafficking and signaling: journey to the cross roads. *Front. Immunol.* **11**, 615603
15. Banninger, G., and Reich, N. C. (2004) STAT2 nuclear trafficking. *J. Biol. Chem.* **279**, 39199–39206
16. Shuai, K., Horvath, C. M., Huang, L. H., Qureshi, S. A., Cowburn, D., and Darnell, J. E. (1994) Interferon activation of the transcription factor Stat91 involves dimerization through SH2-phosphotyrosyl peptide interactions. *Cell* **76**, 821–828
17. Wang, Y., Song, Q., Huang, W., Lin, Y., Wang, X., Wang, C., *et al.* (2021) A virus-induced conformational switch of STAT1-STAT2 dimers boosts antiviral defenses. *Cell Res.* **31**, 206–218
18. Philips, R. L., Wang, Y., Cheon, H., Kanno, Y., Gadina, M., Sartorelli, V., *et al.* (2022) The JAK-STAT pathway at 30: much learned, much more to do. *Cell* **185**, 3857–3876
19. Platanitis, E., Demiroz, D., Schneller, A., Fischer, K., Capelle, C., Hartl, M., *et al.* (2019) A molecular switch from STAT2-IRF9 to ISGF3 underlies interferon-induced gene transcription. *Nat. Commun.* **10**, 2921
20. Meyer, T., and Vinkemeier, U. (2004) Nucleocytoplasmic shuttling of STAT transcription factors. *Eur. J. Biochem.* **271**, 4606–4612
21. Ran, Y., Li, D., Xiong, M.-G., Liu, H.-N., Feng, T., Shi, Z.-W., *et al.* (2022) African swine fever virus I267L acts as an important virulence factor by inhibiting RNA polymerase III-RIG-I-mediated innate immunity. *PLoS Pathog.* **18**, e1010270
22. Huang, L., Li, J., Zheng, J., Li, D., and Weng, C. (2022) Multifunctional pMGF505-7R is a key virulence-related factor of African swine fever virus. *Front. Microbiol.* **13**, 852431
23. Zheng, X., Nie, S., and Feng, W.-H. (2022) Regulation of antiviral immune response by African swine fever virus (ASFV). *Virol. Sin.* **37**, 157–167
24. García-Belmonte, R., Pérez-Núñez, D., Pittau, M., Richt, J. A., and Revilla, Y. (2019) African swine fever virus Armenia/07 virulent strain controls interferon beta production through the cGAS-STING pathway. *J. Virol.* **93**, e02298-18
25. Bosch-Camós, L., López, E., and Rodriguez, F. (2020) African swine fever vaccines: a promising work still in progress. *Porcine Health Manag.* **6**, 17
26. Zhang, K., Yang, B., Shen, C., Zhang, T., Hao, Y., Zhang, D., *et al.* (2022) MGF360-9L is a major virulence factor associated with the African swine fever virus by antagonizing the JAK/STAT signaling pathway. *mBio* **13**, e0233021
27. Huang, Z., Cao, H., Zeng, F., Lin, S., Chen, J., Luo, Y., *et al.* (2023) African swine fever virus MGF505-7R interacts with interferon regulatory factor 9 to evade the type I interferon signaling pathway and promote viral replication. *J. Virol.* **97**, e0197722
28. Ding, M., Dang, W., Liu, H., Xu, F., Huang, H., Sunkang, Y., *et al.* (2022) Combinational deletions of MGF360-9L and MGF505-7R attenuated highly virulent African swine fever virus and conferred protection against homologous challenge. *J. Virol.* **96**, e0032922
29. Huang, Z., Xu, Z., Cao, H., Zeng, F., Wang, H., Gong, L., *et al.* (2022) A triplex PCR method for distinguishing the wild-type African swine fever virus from the deletion strains by detecting the gene insertion. *Front. Vet. Sci.* **9**, 921907
30. Samuel, C. E. (2001) Antiviral actions of interferons. *Clin. Microbiol. Rev.* **14**, 778–809
31. Shemesh, M., Lochte, S., Piehler, J., and Schreiber, G. (2021) IFNAR1 and IFNAR2 play distinct roles in initiating type I interferon-induced JAK-STAT signaling and activating STATs. *Sci. Signal.* **14**, eabe4627
32. Walter, M. R. (2020) The role of structure in the biology of interferon signaling. *Front. Immunol.* **11**, 606489
33. Kisseleva, T., Bhattacharya, S., Braunstein, J., and Schindler, C. W. (2002) Signaling through the JAK/STAT pathway, recent advances and future challenges. *Gene* **285**, 1–24
34. Li, X., Leung, S., Qureshi, S., Darnell, J. E., and Stark, G. R. (1996) Formation of STAT1-STAT2 heterodimers and their role in the activation of IRF-1 gene transcription by interferon-alpha. *J. Biol. Chem.* **271**, 5790–5794
35. Haque, S. J., and Williams, B. R. (1994) Identification and characterization of an interferon (IFN)-stimulated response element-IFN-stimulated gene factor 3-independent signaling pathway for IFN-alpha. *J. Biol. Chem.* **269**, 19523–19529
36. Li, D., Zhang, J., Yang, W., Li, P., Ru, Y., Kang, W., *et al.* (2021) African swine fever virus protein MGF-505-7R promotes virulence and pathogenesis by inhibiting JAK1- and JAK2-mediated signaling. *J. Biol. Chem.* **297**, 101190
37. Liu, H., Zhu, Z., Feng, T., Ma, Z., Xue, Q., Wu, P., *et al.* (2021) African swine fever virus E120R protein inhibits interferon beta production by interacting with IRF3 to block its activation. *J. Virol.* **95**, e0082421
38. Riera, E., Pérez-Núñez, D., García-Belmonte, R., Miorin, L., García-Sastre, A., and Revilla, Y. (2021) African swine fever virus induces STAT1 and STAT2 degradation to counteract IFN-I signaling. *Front. Microbiol.* **12**, 722952
39. Li, L., Fu, J., Li, J., Guo, S., Chen, Q., Zhang, Y., *et al.* (2022) African swine fever virus pI215L inhibits type I interferon signaling by targeting interferon regulatory factor 9 for autophagic degradation. *J. Virol.* **96**, e0094422
40. Xu, Z., Hu, Y., Li, J., Wang, A., Meng, X., Chen, L., *et al.* (2023) Screening and identification of the dominant antigens of the African swine fever virus. *Front. Vet. Sci.* **10**, 1175701
41. Gothe, F., Stremenova Spegarova, J., Hatton, C. F., Griffin, H., Sargent, T., Cowley, S. A., *et al.* (2022) Aberrant inflammatory responses to type I interferon in STAT2 or IRF9 deficiency. *J. Allergy Clin. Immunol.* **150**, 955–964.e16
42. Green, D. S., Young, H. A., and Valencia, J. C. (2017) Current prospects of type II interferon γ signaling and autoimmunity. *J. Biol. Chem.* **292**, 13925–13933
43. Reid, S. P., Leung, L. W., Hartman, A. L., Martinez, O., Shaw, M. L., Carbonnelle, C., *et al.* (2006) Ebola virus VP24 binds karyopherin alpha1 and blocks STAT1 nuclear accumulation. *J. Virol.* **80**, 5156–5167
44. Warnking, K., Klemm, C., Löffler, B., Niemann, S., van Krüchten, A., Peters, G., *et al.* (2015) Super-infection with *S taphylococcus aureus* inhibits influenza virus-induced type I IFN signalling through impaired STAT1-STAT2 dimerization. *Cell Microbiol.* **17**, 303–317
45. Sun, M., Yu, S., Ge, H., Wang, T., Li, Y., Zhou, P., *et al.* (2022) The A137R protein of African swine fever virus inhibits type I interferon production *via* the autophagy-mediated lysosomal degradation of TBK1. *J. Virol.* **96**, e0195721
46. Li, D., Yang, W., Li, L., Li, P., Ma, Z., Zhang, J., *et al.* (2021) African swine fever virus MGF-505-7R negatively regulates cGAS-STING-mediated signaling pathway. *J. Immunol.* **206**, 1844–1857
47. Huang, L., Chen, W., Liu, H., Xue, M., Dong, S., Liu, X., *et al.* (2023) African swine fever virus HLJ/18 CD2v suppresses type I IFN production and IFN-stimulated genes expression through negatively regulating cGMP-AMP synthase-STING and IFN signaling pathways. *J. Immunol.* **210**, 1338–1350
48. Malmquist, W. A., and Hay, D. (1960) Hemadsorption and cytopathic effect produced by African Swine Fever virus in swine bone marrow and buffy coat cultures. *Am. J. Vet. Res.* **21**, 104–108